HHS Public Access

Author manuscript

*Neuron*. Author manuscript; available in PMC 2017 October 19.

Published in final edited form as:

*Neuron*. 2016 October 19; 92(2): 479–492. doi:10.1016/j.neuron.2016.09.040.

# Presynaptic protein synthesis is required for long-term plasticity of GABA release

**Thomas J. Younts**[1,5,6,*], **Hannah R. Monday**[1,5], **Barna Dudok**[3,4], **Mathew E. Klein**[1], **Bryen A. Jordan**[1,2], **István Katona**[3], and **Pablo E. Castillo**[1,7,*]

[1]Dominick P. Purpura Department of Neuroscience, Albert Einstein College of Medicine, New York, USA

[2]Department of Psychiatry and Behavioral Sciences, Albert Einstein College of Medicine, New York, USA

[3]Momentum Laboratory of Molecular Neurobiology, Institute of Experimental Medicine, Hungarian Academy of Sciences, Budapest, Hungary

[4]School of Ph.D. Studies, Semmelweis University, Budapest, Hungary

## Summary

Long-term changes of neurotransmitter release are critical for proper brain function. However, the molecular mechanisms underlying these changes are poorly understood. While protein synthesis is crucial for the consolidation of postsynaptic plasticity, whether and how protein synthesis regulates presynaptic plasticity in the mature mammalian brain remains unclear. Here, using paired whole-cell recordings in rodent hippocampal slices, we report that presynaptic protein synthesis is required for long-term, but not short-term, plasticity of GABA release from type-1 cannabinoid receptor ($CB_1$)-expressing axons. This long-term depression of inhibitory transmission (iLTD) involves cap-dependent protein synthesis in presynaptic interneuron axons but not somata. Translation is required during the induction, but not maintenance, of iLTD. Mechanistically, $CB_1$ activation enhances protein synthesis via the mTOR pathway. Furthermore, using super-resolution STORM microscopy, we revealed eukaryotic ribosomes in $CB_1$-expressing axon terminals. These findings suggest that presynaptic local protein synthesis controls neurotransmitter release during long-term plasticity in the mature mammalian brain.

[*]Correspondence: Pablo E. Castillo, M.D., Ph.D., Dominick P. Purpura Department of Neuroscience, Albert Einstein College of Medicine, Rose F. Kennedy Center, Room 703, 1410 Pelham Parkway South, Bronx, NY 10461, USA, Phone: +1.718.430.3262, pablo.castillo@einstein.yu.edu, Thomas J. Younts, Ph.D., Phone: +44.020.7679.3214, t.younts@ucl.ac.uk.

[5]Co-first author

[6]Present Address: Department of Neuroscience, Physiology and Pharmacology, University College London, Gower Street, London WC1E 6BT, UK

[7]Lead Contact



Author Contributions: TJY, MEK, and PEC conceived and TJY and PEC directed the project. TJY, HRM and MEK performed electrophysiology and analyzed data; TJY performed cell paired recordings and two-photon microscopy; HRM performed second-harmonic generation microscopy; MEK performed PCR; HRM and BAJ performed FUNCAT; BD and IK performed STORM microscopy and analyzed data. TJY and PEC wrote and all authors reviewed and edited the manuscript.

There are no conflicts of interest.

## Introduction

Long-term plasticity of neurotransmitter release critically regulates circuit function (Castillo, 2012). Despite decades of research, the molecular basis of long-term changes in neurotransmitter release remains unsolved. While synthesis of new protein is required for stabilizing synapses during postsynaptically-expressed forms of long-term plasticity (e.g. long-term potentiation; LTP and long-term depression; LTD) (Buffington et al., 2014; Santini et al., 2014), whether and how presynaptic protein synthesis is involved in long-term presynaptic plasticity in the mature mammalian brain is unclear. Resolving this issue is important because LTP and LTD are linked to cognition, and dysregulated translation during long-term plasticity is associated with autism, Fragile X Syndrome, and Alzheimer Disease (Buffington et al., 2014; Darnell and Klann, 2013; Santini et al., 2014).

Presynaptic local protein synthesis, a process whereby mRNAs are translated in axons and terminals, can endow remote neuronal compartments with the flexibility to rapidly respond to local synaptic activity, independent of the soma (Alvarez et al., 2000). Although ribosomes have routinely been documented in mammalian axonal growth cones during early embryonic development, as well as in regenerating, cultured, and peripheral sensory axons (for recent reviews, see Crispino et al., 2014; Gomes et al., 2014; Holt and Schuman, 2013; Jung et al., 2014), the prevailing view is that fully developed axons in the healthy mammalian brain are incapable of supporting protein synthesis. In non-mammalian preparations, where translation inhibitors can be injected into relatively large axons, a role for local protein synthesis during long-term plasticity has been established (Beaumont et al., 2001; Martin et al., 1997; Zhang and Poo, 2002). Mammalian central nervous system (CNS) axons are considerably smaller and therefore, more difficult to experimentally manipulate. To date, a direct demonstration for a requirement for presynaptic protein synthesis during long-term plasticity in an intact mammalian CNS circuit is lacking. Moreover, there is very little evidence for the presence of ribosomes inside fully developed presynaptic axon terminals.

One of the most ubiquitously expressed forms of presynaptic plasticity in the mature CNS is mediated by retrograde endocannabinoid (eCB) signaling (Castillo et al., 2012; Kano et al., 2009). eCBs are lipids mobilized by postsynaptic activity that travel backward across the synapse and bind presynaptic $G_{i/o}$-coupled type-1 cannabinoid ($CB_1$) receptors to suppress neurotransmitter release. In the hippocampus, $CB_1$ receptors are highly expressed on GABAergic inhibitory interneuron axon terminals where they mediate both short-term and long-term plasticity. Short-term plasticity in the form of depolarization-induced suppression of inhibition (DSI) typically lasts less than a minute and is likely due to a transient reduction of presynaptic calcium influx (Kano et al., 2009). Long-term depression of inhibition (iLTD) involves more sustained $CB_1$ activation (Chevaleyre and Castillo, 2003), downregulation of PKA (Chevaleyre et al., 2007), and a long-lasting reduction in GABA release. How eCBs control neurotransmitter release during long-term plasticity is incompletely understood. Although striatal eCB-LTD was reported to involve translation (Adermark et al., 2009; Yin et al., 2006) but see (Jung et al., 2012), the mechanism that triggers protein synthesis

remains unknown. Furthermore, direct evidence that $CB_1$ activation leads to protein synthesis is unavailable.

To determine the role of presynaptic protein synthesis in iLTD, we performed long-term paired electrophysiological recordings on synaptically connected inhibitory interneurons and CA1 pyramidal cells in acute rodent hippocampal slices, where local microcircuits are intact. Using single-cell manipulations to block protein translation, we found that iLTD requires protein synthesis exclusively in presynaptic interneurons, most likely in axons. We also show that $CB_1$ activation increases protein synthesis in an mTOR-dependent manner, and that iLTD involves cap-dependent translation. Moreover, using stochastic optical reconstruction microscopy (STORM), we provide evidence that eukaryotic ribosomes are localized inside $CB_1$-expressing interneuron axon terminals. Our findings establish that presynaptic protein synthesis controls neurotransmitter release during long-term plasticity in the mature mammalian CNS.

## Results

### Long-term, but not short-term, eCB-mediated plasticity requires protein synthesis

To assess if eCB-mediated iLTD involves protein synthesis, we first elicited heterosynaptic iLTD (Chevaleyre and Castillo, 2003) by theta-burst stimulation (TBS) of presynaptic inputs onto whole-cell voltage clamped CA1 pyramidal cells in acute hippocampal slices. Compared with interleaved controls, acute bath application of either cycloheximide or anisomycin, two mechanistically distinct inhibitors of eukaryotic ribosome peptide elongation, impaired iLTD (Figure 1A). iLTD can also be triggered with postsynaptic activity such as multiple episodes of DSI (mDSI) (Younts et al., 2013). Compared with controls, acute bath application, but not postsynaptic loading of cycloheximide (Yin et al., 2006) or anisomycin, blocked mDSI-iLTD (Figure 1B), suggesting that postsynaptic translation is dispensable for iLTD. Neither cycloheximide nor anisomycin affected the magnitude or duration of short-term plasticity triggered with DSI (Figure 1C,D), indicating that eCB release and $CB_1$ activation properly function when blocking protein synthesis. Using fluorescent non-canonical amino acid tagging (FUNCAT), a technique that permits visualization of newly synthesized proteins (Dieterich et al., 2010), we confirmed that cycloheximide and anisomycin block translation in slices (Figure 1E,F). Taken together, these results show that protein translation is essential for long-term, but not short-term, inhibitory plasticity.

### Protein synthesis is required for the induction, but not maintenance, of iLTD

Bypassing eCB production and directly activating presynaptic $CB_1$ with the selective agonist WIN 55,212-2 (WIN) induces chemical-iLTD (Chevaleyre and Castillo, 2003; Chevaleyre et al., 2007; Heifets et al., 2008). Using extracellular field inhibitory postsynaptic potential (fIPSP) recordings from the cell body layer, we found that WIN paired with presynaptic activity triggered iLTD (Heifets et al., 2008), which was expressed presynaptically as reflected by an increased paired-pulse ratio (i.e. reduced release probability, $P_r$) (Figure 2A). Cycloheximide or anisomycin abolished iLTD and the associated change in $P_r$ (Figure 2A). To address whether translation is necessary for the induction or maintenance of iLTD, we

acutely exposed slices to cycloheximide during or after $CB_1$ activation and found that protein synthesis was not required during the maintenance-phase of iLTD (Figure 2B). Neither cycloheximide nor anisomycin affected basal inhibitory synapse strength (Figure 2C), indicating that protein synthesis is specifically required for long-term plasticity, and that constitutive protein synthesis does not significantly alter GABA release. As expected, iLTD was prevented in slices exposed to the selective $CB_1$ inverse agonist/antagonist AM251 or SR 141716 (Figure 2D). We also examined the potential contribution of mRNA transcription to iLTD. iLTD remained intact when transcription was blocked with actinomycin-D (Figure S1A), and actinomycin-D efficacy was confirmed using RT-PCR in slices (Figure S1B). Collectively, these findings indicate that protein synthesis, and not transcription, is required for the induction, but not maintenance, of iLTD.

## $CB_1$ activation enhances protein translation

Given that $CB_1$-mediated iLTD requires protein synthesis, we next tested whether $CB_1$ activation can promote translation. To increase the likelihood of detecting and quantifying potential $CB_1$-mediated changes in protein synthesis, we used FUNCAT on cultured primary hippocampal neurons. Cultured neurons mainly express $CB_1$ in axons, but unlike inhibitory interneurons *in situ*, they also express $CB_1$ in soma and dendrites (Irving et al., 2000; Twitchell et al., 1997). Using MAP2 labeling to identify neurons, we found that WIN increased translation (Figure 3A,B). Co-application of WIN with AM251 abolished this effect (Figure 3A,B), indicating that $CB_1$ activation triggered translation. AM251 treatment alone did not significantly change the FUNCAT signal (Figure 3A,B), suggesting that basal $CB_1$ signaling is not coupled to protein synthesis. As expected, the WIN-induced increase in FUNCAT signal was greatly reduced by cycloheximide. Using the selective agonist DHPG, we confirmed that group I metabotropic glutamate receptors (mGluRs) engage protein synthesis (Huber et al., 2000), indicating the FUNCAT assay worked as intended. We also assessed protein translation in $CB_1$-expressing axons and found that the FUNCAT signal in the presence of WIN was reduced by AM251 (Figure 3C). We conclude that neuronal $CB_1$ activation increases newly synthesized protein in neurons and axons.

## Presynaptic $CB_1$-mediated iLTD requires mTOR signaling and cap-dependent translation

$CB_1$ can signal via the mammalian target of rapamycin (mTOR), p38 mitogen-activated protein kinase (MAPK), and/or MAPK/extracellular signal-regulated kinase (ERK) pathways (Howlett et al., 2002). Each of these pathways is known to regulate protein synthesis and play a role in postsynaptic forms of LTP and LTD (Buffington et al., 2014; Santini et al., 2014). To test if $CB_1$ activation increases protein synthesis in an mTOR-dependent manner, we measured translation using FUNCAT in primary neurons and found that the mTOR selective inhibitor torin-2 abolished the WIN-induced increase in translation (Figure 4A,B). Application of torin-2 alone had no significant effect on protein synthesis suggesting that mTOR does not regulate constitutive protein synthesis (Figure 4A,B). To examine whether mTOR plays a role in iLTD, we triggered iLTD in acute hippocampal slices. Compared with interleaved controls, torin-2 abolished synaptically (Figure 4C) and chemically-induced iLTD (Figure 4D). Similar to protein synthesis (Figure 2B), mTOR signaling was required during the induction, but not maintenance, of iLTD (Figure 4D). Notably, torin-2 alone did not affect basal inhibitory synapse strength (104.5 ± 2.2% of

baseline, n = 4, p = 0.19735, paired t-test, data not shown), suggesting that constitutive mTOR signaling does not modify basal GABA release. In addition, a different mTOR inhibitor, rapamycin, impaired iLTD (Figure 4E). We further examined the contribution of cap-dependent protein synthesis to iLTD. Chemical-iLTD was blocked in slices exposed to 4EGI-1 (Figure 4E), which disrupts the eukaryotic initiation factor 4F (eIF4F) complex at the level of eIF4E and eIF4G (Moerke et al., 2007), as well as ISRIB (Figure 4E), which interferes with translation initiation by preventing the effects of phosphorylated eIF2α (Sekine et al., 2015). Neither 4EGI-1 nor ISRIB alone had a significant effect on basal inhibitory fIPSP amplitude (4EGI-1: 106.4 ± 8.0% of baseline, n = 4; p = 0.48092, paired t-test; ISRIB: 96.2 ± 2.6% of baseline, n = 7, p = 0.1974, paired t-test, data not shown), further signifying that the effects of blocking translation were specific to long-term plasticity. We found a partial block of iLTD in slices treated with the p38 MAPK inhibitor SB 202190 whereas the ERK/MAPK inhibitor U-0126 had no effect (Figure 4E). Collectively, our results demonstrate that $CB_1$ activation drives protein synthesis in an mTOR-dependent manner and that cap-dependent translation is essential for iLTD.

## Presynaptic, but not postsynaptic, cap-dependent translation is critical for iLTD

To directly test a role for presynaptic protein synthesis in iLTD at the single-cell level, we performed long-term paired electrophysiological recordings (up to 5 hrs) between individual hippocampal interneurons and CA1 pyramidal cells. Paired recordings allow independent control over presynaptic and postsynaptic signaling, thereby providing a means to study neurotransmitter release from fully developed GABAergic synaptic terminals in an intact circuit. Protein synthesis was inhibited at the single-cell level using the small molecule, membrane impermeable inhibitor, $M^7GpppG$ (M7). M7 is an mRNA cap analog that competes with endogenous 7-methyl guanosine 5'-capped mRNAs for binding to eIF4E, one of several proteins comprising the eIF4F complex that regulates cap-dependent translation (Sonenberg and Hinnebusch, 2009). Excess M7 has been used previously to disrupt translation-dependent forms of long-term plasticity (Beaumont et al., 2001; Huber et al., 2000). To test whether iLTD requires presynaptic protein synthesis, M7 was loaded via the patch pipette directly into regular-spiking, DSI-sensitive and therefore $CB_1$-expressing interneurons (Figure 5A). Remarkably, loading M7 presynaptically for >1 hr abolished iLTD (Figure 5B,C, Figure S2A). We quantified GABA release during the baseline and after inducing iLTD in three ways: neurotransmitter release probability ($P_r$; calculated as the number of synaptic release events, i.e. the inverse failure rate); synaptic efficacy (a measure of synaptic strength calculated by averaging all synaptic events including responses and failures); and synaptic potency (which is the average of only synaptic responses). $P_r$, synaptic efficacy (Figure 5B,C), and potency (baseline: 34.5 ± 12.8 pA vs. after iLTD induction: 31.8 ± 11.0 pA, n = 6; p = 0.50625, paired t-test, data not shown) remained stable (for up to 3 hrs) after attempting to induce iLTD. These results reinforce the idea that disrupting constitutive presynaptic protein synthesis does not alter basal GABA release. M7 did not alter physiological parameters of interneurons such as resting membrane potential (M7 loaded presynaptically: −62.9 ± 1.9 mV vs. M7 not loaded presynaptically: −62.1 ± 1.8 mV; p = 0.73584, unpaired t-test, n = 6 each) or input resistance (M7 loaded presynaptically: 275.4 ± 42.0 MΩ vs. M7 not loaded presynaptically: 231.5 ± 51.5 MΩ; p = 0.52464, unpaired t-test, n = 6 each). These results establish that presynaptic protein synthesis is

critical for iLTD, and further support a mechanism involving cap-dependent protein synthesis.

To examine the contribution of postsynaptic translation to presynaptic plasticity, M7 was loaded into CA1 pyramidal cells. As predicted, iLTD remained intact (Figure 5D–F, Figure S2A). The magnitude of iLTD, reflected in the $P_r$ and synaptic efficacy measurements, was not significantly different from our previous experiments in which M7 was not present (Younts et al., 2013). Consistent with multivesicular release from these terminals (Biro et al., 2006), synaptic potency also was reduced (baseline: 34.5 ± 11.7 pA vs. after iLTD induction: 16.8 ± 6.0 pA, n = 6, p = 0.03423, paired t-test, data not shown). These experiments indicate that iLTD does not “washout” of presynaptic or postsynaptic compartments because iLTD was induced in recordings in which the baseline exceeded 1 hr. Notably, iLTD was still $CB_1$-dependent when postsynaptic translation was blocked with M7 (Figure S2B), signifying that blocking *post*synaptic protein synthesis does not alter eCB production or $CB_1$ signaling required for inducing iLTD. To validate that M7 worked as intended, we assessed the well-characterized, protein synthesis-dependent mGluR-LTD at excitatory Schaffer collateral-to-CA1 pyramidal cell synapses (Huber et al., 2000), and found that mGluR-LTD, triggered chemically with DHPG, was not observed when M7 was loaded postsynaptically for ~30 min (Figure S2C). These results demonstrate that postsynaptic translation is dispensable for iLTD.

## Somatic protein synthesis in presynaptic interneurons is dispensable for iLTD

Given that $CB_1$ is predominantly localized to hippocampal interneuron axons and terminals *in situ* (Dudok et al., 2015; Katona et al., 1999), that iLTD is expressed presynaptically as reduced GABA release (Castillo et al., 2012), and that loading M7 into interneurons blocked iLTD (Figure 5A–C, Figure S2A), we hypothesized that translation is required locally in axons and/or terminals that are remote from the interneuron cell body. Consistent with this hypothesis, we found a significant positive correlation between the amount of time M7 was loaded presynaptically and the likelihood of blocking iLTD (Figure S3A), suggesting M7 must diffuse into remote axonal compartments to exert its blocking effect. For the experiments in which M7 was omitted from the presynaptic interneuron, the magnitude of iLTD remained stable and no correlation was observed (Figure S3A). To determine if M7 can diffuse into remote axons at times matching iLTD block, we used two-photon fluorescence microscopy to track the diffusion of two fluorescent molecules, Alexa Fluor-594 and Lucifer yellow, which are similar in size to M7 (i.e. M7 proxies). We readily detected M7 proxies in putative axons (Figure S3B,C). To test the hypothesis that somatic translation in interneurons is dispensable for iLTD, we performed paired recordings and loaded the type-1 ribosome inactivating toxin, gelonin, which irreversibly interferes with protein elongation, into regular-spiking, DSI-sensitive interneurons. Given its relatively large size (~30 kDa), we reasoned that gelonin introduced via the patch pipette would be relatively restricted to the soma and proximal neurites and therefore less effective at blocking translation in distal axon terminals. We could only detect gelonin (3–30 μM, labeled with Alexa Fluor-488) in somata and proximal dendrites but not in putative axons (Figure S3B,C). Functionally, gelonin (3 μM) loaded presynaptically for 105.3 ± 4.9 min failed to block iLTD (Figure 6A,B). To assess if gelonin blocked somatic translation, we

loaded gelonin (3 μM) for ~30 min into one of two neighboring CA1 interneurons in slices and performed FUNCAT (Figure 6C,D). Gelonin substantially reduced somatic translation in these interneurons (Figure 6C,D). As a functional positive control in interleaved experiments, we found that gelonin (3 μM) loaded postsynaptically for ~30 min readily blocked mGluR-LTD at excitatory synapses onto CA1 pyramidal cells (Figure 6E). Finally, we examined the possibility that a somatically synthesized protein might traffic along microtubules into axonal compartments during iLTD. Slices were pre-incubated and continuously perfused with the microtubule depolymerizing agent colchicine (for up to 5 hrs) or nocodazole (for up to 8 hrs). These reagents had no effect on iLTD (Figure 6F) or intrinsic membrane properties (Figure S4A), despite nocodazole disrupting neuronal microtubule integrity in slices as measured with second harmonic generation microscopy (Figure S4B,C). These observations suggest that microtubule-based trafficking mechanisms do not participate in iLTD. Taken together, these results indicate that somatic translation and transport are not required for iLTD, strongly suggesting that iLTD involves presynaptic protein synthesis in axons.

## Anatomical evidence for ribosomes in mature mammalian axon terminals

If iLTD involves presynaptic protein synthesis, then ribosomes should be present in $CB_1$-expressing interneuron axons and terminals. To visualize ribosomes specifically within this interneuron type, we co-immunostained mouse and rat hippocampal slices using antibodies specific for $CB_1$ and ribosomes. We and others have previously validated the $CB_1$ antibody (Dudok et al., 2015; Fukudome et al., 2004). The Y10b antibody is also well-characterized and validated, recognizing 5.8S non-coding ribosomal RNA in the 60S subunit. Consistent with previous reports (Dudok et al., 2015; Katona et al., 1999), confocal imaging revealed a characteristically dense network of $CB_1$-expressing basket-like axons and preterminal axon segments encircling $CB_1$-immunonegative CA1 pyramidal cell bodies (Figure 7A, Figure S5A). As expected, there was high ribosome density expressed in the perinuclear cytoplasm of CA1 pyramidal cell bodies (Figure 7A, Figure S5A). With the exception of nucleoli (not shown), where 5.8S rRNA is made and spliced, the nucleus was nearly devoid of 5.8S rRNA. We validated Y10b staining by treating sections with RNAse A and micrococcal nuclease enzymes, which degrade RNA and thus the Y10b epitope. Compared with control, sections pretreated with nucleases had substantially less Y10b labeling (Figure 7A, Figure S5A,B).

In an effort to detect ribosomes in $CB_1$-expressing axon terminals, we performed 3D STORM imaging (Huang et al., 2008). Using a recently developed combined STORM/confocal imaging approach that reliably measures $CB_1$ position in the plasma membrane (Barna et al., 2016; Dudok et al., 2015), we visualized 5.8S rRNA molecules within $CB_1$-expressing axon terminals (Figure 7B) located in the somatic and dendritic fields of CA1 (Figure S5B). Nuclease pretreatment largely eliminated 5.8S rRNA immunostaining from these terminals (Figure 7A,D, Figure S5B). In a complementary set of experiments, we immunolabeled ribosomal protein S6 (rpS6), which is an integral component of the eukaryotic 40S ribosomal subunit and an effector of mTOR signaling. rpS6 molecules were also readily visualized with STORM imaging inside $CB_1$-expressing axon terminals (Figure 7C, Figure S5C). The densities of 5.8S rRNA (Figure 7D) and rpS6 protein (Figure 7E)

puncta were significantly higher (by ~90%) in axon terminals compared to the corresponding background signal measured from CA1 pyramidal cell nuclei. Preterminal axon segments exhibited an intermediate labeling density. Quantitative nanoscale analysis showed an identical clustering distribution for 5.8S rRNA and rpS6 localization points within $CB_1$-expressing axon terminals (Figure 7F), and dual channel STORM revealed co-clustering of 5.8S rRNA and rpS6 molecules in these boutons (Figure S6A–C). The mean number (± standard deviation) of 5.8S rRNA and rpS6 clusters per bouton was 3.34 ± 0.79 and 2.92 ± 1.16, and the percentage of ribosome-containing boutons was 91 ± 7% and 83 ± 18%, respectively. As expected, $CB_1$-expressing axon terminals containing the presynaptic active zone protein bassoon also showed ribosomal labeling (Figure S6D–G). Presynaptic 5.8S rRNA STORM signal was observed in $CB_1$-expressing axon terminals from rat hippocampal sections, and signal specificity was confirmed in nuclease-treated sections (control, n = 57 boutons vs. nuclease treatment, n = 56 boutons, 2 animals each, $p < 0.0001$, Mann-Whitney U test, data not shown). Interestingly, presynaptic ribosomal labeling was also detected in parvalbumin-positive inhibitory interneuron boutons (Figure S7). The number of 5.8S rRNA and rpS6 clusters per bouton was 2.41 ± 0.84 and 2.42 ± 1.03, and the percentage of ribosome-containing boutons was 82 ± 11% and 77 ± 14%, respectively. Jointly, these data provide strong anatomical support for eukaryotic ribosomes in mammalian axon terminals of inhibitory interneurons.

To determine the nanodomain distribution of ribosomes within presynaptic $CB_1$-expressing interneuron terminals, we employed dual-channel 3D directSTORM imaging. We previously established that $CB_1$ localization points, which delimit the presynaptic bouton, can be fit with a convex hull with nanoscale precision (Dudok et al., 2015), thereby defining the membrane of the axon terminal (Figure 7H). Dual-STORM imaging uncovered 5.8S rRNA within $CB_1$-expressing axon terminals (Figure 7G,H). Quantitative nanoscale distribution analysis uncovered a high density of 5.8S rRNA within the presynaptic terminal just inside the plasma membrane (Figure 7G, Figure S6D–G). The density of 5.8S rRNA just outside the presynaptic plasma membrane, corresponding to the synaptic cleft and interstitial space, was virtually zero (Figure 7G). Taken together, these findings provide molecular and anatomical evidence for the presence of presynaptic ribosomes inside $CB_1$-expressing interneuron terminals.

## Discussion

We established that presynaptic protein synthesis is essential for a presynaptically-expressed form of long-term plasticity in the mature mammalian brain. We found that $CB_1$ activation generates new proteins, and that iLTD likely requires axonal protein synthesis independent of somatic translation, transcription, and microtubule-based trafficking mechanisms. Our combined molecular and anatomical approach revealed eukaryotic ribosomes in fully-developed $CB_1$-expressing interneuron axon terminals. Mechanistically, $CB_1$ activation drives the cap-dependent translation machinery via the mTOR pathway. Translation plays a specific role in long-term plasticity since disrupting translation initiation or peptide elongation did not affect basal GABA release or short-term plasticity. We also report that protein synthesis is required for the induction, but not maintenance, of iLTD. These findings

converge on a novel model whereby presynaptically synthesized proteins act as a molecular switch to persistently reduce GABA release from inhibitory interneuron terminals.

Neurons must coordinate gene expression at thousands of synapses distant from their soma. Local translation can impart axons and dendrites with computational autonomy to rapidly respond to the environment, independent of the soma (Alvarez et al., 2000; Holt and Schuman, 2013; Jung et al., 2014). The concept of local presynaptic protein synthesis was first proposed nearly 50 years ago (for a thorough review, see Alvarez et al., 2000). Presynaptic local protein synthesis during long-term plasticity has since been demonstrated in non-mammalian preparations such as crayfish (Beaumont et al., 2001), sea slug (Martin et al., 1997), frog (Zhang and Poo, 2002), and leech (Yuan and Burrell, 2013). An advantage of these preparations is that the presynaptic axons are relatively large and can be directly manipulated via pressure-injection of translation inhibitors. In contrast, mammalian axons are much smaller and therefore more difficult to access. Previous research in rodents has so far relied on non-physiological treatments such as axotomy or non-specific manipulations such as blocking postsynaptic protein synthesis to infer a role for presynaptic translation during long-term plasticity (Barnes et al., 2010; Calixto et al., 2003; Hagena and Manahan-Vaughan, 2013; Huang and Hsu, 2004; Huang et al., 1994; Kelly et al., 2000; Yin et al., 2006). Protein synthesis can be upregulated in response to injury or occur in neighboring neurons or glia. We used long-term paired recordings and single-cell manipulations in a locally intact circuit to demonstrate that presynaptic, likely axonal, protein synthesis is essential for regulating neurotransmitter release during long-term plasticity. Our findings also indicate that presynaptic protein synthesis during long term-plasticity is evolutionarily conserved from invertebrates to mammals.

The presence of ribosomes has been well documented in mammalian axonal growth cones, regenerating axons, and peripheral sensory axons (Crispino et al., 2014; Jung et al., 2014), However, failure to detect ribosomes in mature mammalian CNS axons (Palay and Palade, 1955), and the observation that neuronal somata can source protein to axons (Droz and Leblond, 1963), likely gave rise to the notion that presynaptic compartments in the mature mammalian brain do not synthesize proteins. This dogma persisted despite ribosomes being identified in axon initial segments of mammalian cortical principal cells (Jones and Powell, 1969; Steward and Ribak, 1986) and spinal nerves (Koenig et al., 2000). Ribosome-associated proteins, initiation and elongation factors have now been detected in whole-brain presynaptic bouton preparations (Wilhelm et al., 2014), and hundreds of mRNA transcripts encoding presynaptic proteins were isolated from cultured cortical axons (Taylor et al., 2009), hippocampal slices of CA1 neuropil (Cajigas et al., 2012), and retinal ganglion cell axons *in vivo* (Shigeoka et al., 2016). In addition, axonal protein synthesis has recently been linked with synaptic transmission and axon maintenance (Shigeoka et al., 2016; Yoon et al., 2012), which may be dysregulated in Alzheimer's disease (Baleriola et al., 2014) and Fragile X Syndrome (Akins et al., 2012; Christie et al., 2009). These studies and ours collectively raise the strong possibility that the soma is not the exclusive origin of presynaptic proteins. Further, our work establishes that presynaptic ribosomes play a functional role in presynaptic long-term plasticity.

Our findings using various protein synthesis inhibitors suggest that presynaptic $CB_1$-expressing interneuron terminals contain eukaryotic ribosomes. We used super-resolution STORM microscopy to provide direct evidence for ribosomes in axonal boutons and to quantify, in a cell-type- and synapse-specific manner, their nanoscale spatial distribution. We found a high density of ribosomes within 25–400 nm of the presynaptic plasma membrane, where they are positioned to integrate $CB_1$ signaling. It is unclear why previous ultrastructural studies in mature CNS axons failed to detect ribosomes in synaptic terminals. Presumably, those studies lacked sufficient sensitivity to detect ribosomes or focused exclusively on excitatory synapses. Alternatively, ribosomes in certain presynaptic terminals may be disassembled and thus go undetected until an external cue (e.g. activity or receptor ligand) initiates translation (Tcherkezian et al., 2010). It is also conceivable that certain presynaptic terminals express unconventional ribosomes (Xue and Barna, 2012). Regardless of the underlying biological or technical explanation, our study demonstrates that eukaryotic ribosomes are present in fully mature CNS inhibitory interneuron terminals.

$CB_1$ can transduce signals to several downstream effectors including voltage-gated $Ca^{2+}$ and $K^+$ channels, PKA, ERK/MAPK, p38-MAPK, and PI3K (Howlett et al., 2002). Many of these signaling cascades were originally characterized in heterologous overexpression systems. Thus, the precise pathways engaged by $CB_1$ in intact preparations remain unclear. A previous study reported that $CB_1$ activation can indirectly upregulate mTOR signaling, presumably in *post*synaptic compartments (Puighermanal et al., 2009). Instead, we found that both synaptically- and chemically-induced iLTD are coupled to mTOR, suggesting that mTOR signaling operates in *pre*synaptic compartments. Using FUNCAT in cultured hippocampal neurons, we also directly showed that $CB_1$ activation leads to new protein synthesis in an mTOR-dependent manner. To our knowledge, this is the first demonstration that $CB_1$ activation causes an overall increase in protein synthesis. Though it is presently not possible to distinguish between a requirement for constitutive and/or *de novo* protein synthesis during forms of plasticity in which target protein(s) remain unidentified, mTOR can control eIF4F-mediated cap-dependent translation initiation, a highly regulated and rate-limiting step (Sonenberg and Hinnebusch, 2009). Given our findings that eIF4F is critical for iLTD, these results imply that $CB_1$ activation enhances the rate of protein synthesis. Novel methods with improved spatiotemporal resolution need to be developed to reveal *de novo* protein synthesis at presynaptic terminals in brain tissue.

Protein synthesis is commonly linked to the maintenance of long-term plasticity (Buffington et al., 2014; Santini et al., 2014). We found that blocking translation right after inducing iLTD had no effect on long-term plasticity. This observation is consistent with our previous work indicating $CB_1$ activation is required during the induction, but not maintenance, of iLTD (Chevaleyre and Castillo, 2003). Given that $CB_1$ receptors enhance translation, the newly synthesized protein(s) may act as a functional molecular switch to inhibit neurotransmitter release and therefore trigger long-term, but not short-term, plasticity. Once the protein(s) are synthesized and iLTD is established, protein translation is no longer required to maintain the synapse in a depressed state (Klein et al., 2015). While additional research is needed to identify exactly which protein(s) are synthesized, candidates include the translation machinery itself, synaptic vesicle-associated signaling proteins, and structural proteins linked with the cytoskeleton, active zone, and intercellular adhesion. There is

evidence that actin can be locally synthesized in axon growth cones, sensory axons, and cultured CNS axons (for reviews, see Gomes et al., 2014; Jung et al., 2014), and that $CB_1$ activation leads to cytoskeletal rearrangements including axon growth cone collapse/expansion (Argaw et al., 2011; Berghuis et al., 2007; Njoo et al., 2015; Roland et al., 2014). Synthesis of a structural/cytoskeletal protein could increase the coupling distance between presynaptic calcium channels and the active zone to efficiently suppress GABA release.

The impact of iLTD manifests at the circuit level. $CB_1$ receptors expressed on the axon terminals of interneurons can persistently gate excitation via somatic and dendritic disinhibition (Basu et al., 2013; Younts et al., 2013). *In vivo* studies suggest that redistribution of inhibitory interneuron spiking and spike-timing can reconfigure ensembles of active hippocampal pyramidal cells in space and time (Dupret et al., 2013; Klausberger et al., 2005). We propose that presynaptic translation in inhibitory interneurons helps orchestrate the excitability of a subset of pyramidal cells in specific circuits established during the learning processes. Given the important role of protein synthesis in cognitive functions (Buffington et al., 2014; Santini et al., 2014), our results also warrant consideration in the context of dysregulated translational control and inappropriately balanced excitation and inhibition. Dysregulated translation in inhibitory interneurons may be an overlooked mechanism in brain disorders (Buffington et al., 2014; Darnell and Klann, 2013).

## Experimental Procedures

See Supplemental Experimental Procedures for detailed methods.

### Slice preparation and electrophysiology

Acute transverse hippocampal slices (400 μm thick) were prepared from male and female (P15–30) Sprague Dawley rats and C57BL/6 mice using standard procedures approved by NIH and Albert Einstein College of Medicine Institutional Animal Care and Use Committee guidelines. Whole-cell voltage and current clamp recordings were performed with an Axon MultiClamp 700B amplifier (signals filtered at 2 kHz and digitized at 5 kHz). Stimulation and acquisition were controlled with custom software (Igor). Stock reagents were prepared according to the manufacturer's recommendation. All experiments were performed in an interleaved fashion. "n" represents number of independent cells or field recordings in slices.

### FUNCAT and image analysis

Acute hippocampal slices (400 μm thick) or primary hippocampal neurons (from E18–19 rats and grown *in vitro* for 18 days) were prepared using standard procedures. Slices were treated with reagents as described and then exposed to azidohomoalanine (AHA) for 2.5 hrs before fixation. Neuron cultures were pre-incubated with methionine-free medium for 30 min, then incubated with AHA for 1.5 hrs and treated with reagents, as described. Following the Click-it® reaction, immunocytochemistry was performed. Images were obtained using the same settings for all samples within an experiment. Experimenter was blind to the treatment condition. Image processing was performed with ImageJ (NIH).

### STORM microscopy and image analysis

Experimental procedures were approved by the Hungarian Committee of the Scientific Ethics of Animal Research. Acute hippocampal slices (300 μm thick) were prepared from male Sprague-Dawley rats and C57BL/6N mice (P30–40) according to standard procedures. Tissue processing, immunostaining, and imaging was performed as described (Barna et al., 2016; Dudok et al., 2015). After data acquisition, the confocal images were deconvolved. Identification of single-molecule localization points was performed with NIS-Elements N-STORM module (Nikon). Correlated analysis of confocal and STORM images was performed in VividSTORM. Localization precision was measured from the standard deviation of coordinates in isolated clusters (Dudok et al., 2015) at 13 nm and 34 nm in the lateral and axial dimensions, respectively. The localization accuracy for determining the position of one blinking event was 6.8 nm with single channel STORM and 10.6 nm with dual-channel STORM. Three-dimensional STORM renderings of localization points were constructed using Visual Molecular Dynamics software. All images within each experiment were processed in parallel using identical imaging and analysis conditions.

### Statistics

Summary data are presented as mean ± standard error of mean (SEM), unless otherwise indicated. Significance ($p < 0.05$) was assessed with one-way ANOVA (means comparison with *post hoc* Bonferroni test for electrophysiology and FUNCAT, or Tukey test for STORM), Student's paired and unpaired t-tests, Wilcoxon matched-pairs signed rank test, Mann Whitney U-test, or Pearson's correlation coefficient, as indicated.

## Supplementary Material

Refer to Web version on PubMed Central for supplementary material.

## Acknowledgments

We thank all Castillo lab members for discussions, Stefano Lutzu and Pablo Lituma for technical assistance with field recordings and two-photon laser imaging, and Carlton Christie for field recordings; Balázs Pintér and Erika Tischler for technical assistance, and Kata Kenesei, Máté Kisfali and Benjamin Barti for slices. We acknowledge Vera DesMarais and David Entenberg at the Einstein Analytical Imaging Facility for help with second harmonic generation microscopy; and László Barna, the Nikon Microscopy Center at the Institute of Experimental Medicine, Nikon Europe B.V., Nikon Austria GmbH, and Auro-Science Consulting Kft for providing STORM microscopy support. We also thank Masahiko Watanabe for antibodies. Supported by the National Institutes of Health (R01-MH081935 and R01-DA17392) to PEC; (R01-NIAAG039521) to BAJ; and (F31-NS073200 and T32-GM007288) to MEK; European Research Council (Grant 243153), Momentum Program (LP2013-54/2013), and Wellcome Trust International Senior Research Fellowship (090946/Z/09/Z) to IK; and in later stages, The Royal Society (Newton International Fellowship) to TJY.

## References

Adermark L, Talani G, Lovinger DM. Endocannabinoid-dependent plasticity at GABAergic and glutamatergic synapses in the striatum is regulated by synaptic activity. Eur J Neurosci. 2009; 29:32–41. [PubMed: 19120438]

Akins MR, Leblanc HF, Stackpole EE, Chyung E, Fallon JR. Systematic mapping of fragile X granules in the mouse brain reveals a potential role for presynaptic FMRP in sensorimotor functions. J Comp Neurol. 2012; 520:3687–3706. [PubMed: 22522693]

Alvarez J, Giuditta A, Koenig E. Protein synthesis in axons and terminals: significance for maintenance, plasticity and regulation of phenotype. With a critique of slow transport theory. Prog Neurobiol. 2000; 62:1–62. [PubMed: 10821981]

Argaw A, Duff G, Zabouri N, Cecyre B, Chaine N, Cherif H, Tea N, Lutz B, Ptito M, Bouchard JF. Concerted action of CB1 cannabinoid receptor and deleted in colorectal cancer in axon guidance. J Neurosci. 2011; 31:1489–1499. [PubMed: 21273433]

Baleriola J, Walker CA, Jean YY, Crary JF, Troy CM, Nagy PL, Hengst U. Axonally synthesized ATF4 transmits a neurodegenerative signal across brain regions. Cell. 2014; 158:1159–1172. [PubMed: 25171414]

Barna L, Dudok B, Miczan V, Horvath A, Laszlo ZI, Katona I. Correlated confocal and super-resolution imaging by VividSTORM. Nat Protoc. 2016; 11:163–183. [PubMed: 26716705]

Barnes SJ, Opitz T, Merkens M, Kelly T, von der Brelie C, Krueppel R, Beck H. Stable mossy fiber long-term potentiation requires calcium influx at the granule cell soma, protein synthesis, and microtubule-dependent axonal transport. J Neurosci. 2010; 30:12996–13004. [PubMed: 20881117]

Basu J, Srinivas KV, Cheung SK, Taniguchi H, Huang ZJ, Siegelbaum SA. A cortico-hippocampal learning rule shapes inhibitory microcircuit activity to enhance hippocampal information flow. Neuron. 2013; 79:1208–1221. [PubMed: 24050406]

Beaumont V, Zhong N, Fletcher R, Froemke RC, Zucker RS. Phosphorylation and local presynaptic protein synthesis in calcium- and calcineurin-dependent induction of crayfish long-term facilitation. Neuron. 2001; 32:489–501. [PubMed: 11709159]

Berghuis P, Rajnicek AM, Morozov YM, Ross RA, Mulder J, Urban GM, Monory K, Marsicano G, Matteoli M, Canty A, et al. Hardwiring the brain: endocannabinoids shape neuronal connectivity. Science. 2007; 316:1212–1216. [PubMed: 17525344]

Biro AA, Holderith NB, Nusser Z. Release probability-dependent scaling of the postsynaptic responses at single hippocampal GABAergic synapses. J Neurosci. 2006; 26:12487–12496. [PubMed: 17135411]

Buffington SA, Huang W, Costa-Mattioli M. Translational control in synaptic plasticity and cognitive dysfunction. Annu Rev Neurosci. 2014; 37:17–38. [PubMed: 25032491]

Cajigas IJ, Tushev G, Will TJ, tom Dieck S, Fuerst N, Schuman EM. The local transcriptome in the synaptic neuropil revealed by deep sequencing and high-resolution imaging. Neuron. 2012; 74:453–466. [PubMed: 22578497]

Calixto E, Thiels E, Klann E, Barrionuevo G. Early maintenance of hippocampal mossy fiber--long-term potentiation depends on protein and RNA synthesis and presynaptic granule cell integrity. J Neurosci. 2003; 23:4842–4849. [PubMed: 12832506]

Castillo PE. Presynaptic LTP and LTD of excitatory and inhibitory synapses. Cold Spring Harb Perspect Biol. 2012:4.

Castillo PE, Younts TJ, Chavez AE, Hashimotodani Y. Endocannabinoid signaling and synaptic function. Neuron. 2012; 76:70–81. [PubMed: 23040807]

Chevaleyre V, Castillo PE. Heterosynaptic LTD of hippocampal GABAergic synapses: a novel role of endocannabinoids in regulating excitability. Neuron. 2003; 38:461–472. [PubMed: 12741992]

Chevaleyre V, Heifets BD, Kaeser PS, Sudhof TC, Castillo PE. Endocannabinoid-mediated long-term plasticity requires cAMP/PKA signaling and RIM1alpha. Neuron. 2007; 54:801–812. [PubMed: 17553427]

Christie SB, Akins MR, Schwob JE, Fallon JR. The FXG: a presynaptic fragile X granule expressed in a subset of developing brain circuits. J Neurosci. 2009; 29:1514–1524. [PubMed: 19193898]

Crispino M, Chun JT, Cefaliello C, Perrone Capano C, Giuditta A. Local gene expression in nerve endings. Dev Neurobiol. 2014; 74:279–291. [PubMed: 23853157]

Darnell JC, Klann E. The translation of translational control by FMRP: therapeutic targets for FXS. Nat Neurosci. 2013; 16:1530–1536. [PubMed: 23584741]

Dieterich DC, Hodas JJ, Gouzer G, Shadrin IY, Ngo JT, Triller A, Tirrell DA, Schuman EM. In situ visualization and dynamics of newly synthesized proteins in rat hippocampal neurons. Nat Neurosci. 2010; 13:897–905. [PubMed: 20543841]

Droz B, Leblond CP. Axonal Migration of Proteins in the Central Nervous System and Peripheral Nerves as Shown by Radioautography. J Comp Neurol. 1963; 121:325–346. [PubMed: 14100019]

Dudok B, Barna L, Ledri M, Szabo SI, Szabadits E, Pinter B, Woodhams SG, Henstridge CM, Balla GY, Nyilas R, et al. Cell-specific STORM super-resolution imaging reveals nanoscale organization of cannabinoid signaling. Nat Neurosci. 2015; 18:75–86. [PubMed: 25485758]

Dupret D, O'Neill J, Csicsvari J. Dynamic reconfiguration of hippocampal interneuron circuits during spatial learning. Neuron. 2013; 78:166–180. [PubMed: 23523593]

Fukudome Y, Ohno-Shosaku T, Matsui M, Omori Y, Fukaya M, Tsubokawa H, Taketo MM, Watanabe M, Manabe T, Kano M. Two distinct classes of muscarinic action on hippocampal inhibitory synapses: M2-mediated direct suppression and M1/M3-mediated indirect suppression through endocannabinoid signalling. Eur J Neurosci. 2004; 19:2682–2692. [PubMed: 15147302]

Gomes C, Merianda TT, Lee SJ, Yoo S, Twiss JL. Molecular determinants of the axonal mRNA transcriptome. Dev Neurobiol. 2014; 74:218–232. [PubMed: 23959706]

Hagena H, Manahan-Vaughan D. Differentiation in the protein synthesis-dependency of persistent synaptic plasticity in mossy fiber and associational/commissural CA3 synapses in vivo. Front Integr Neurosci. 2013; 7:10. [PubMed: 23459947]

Heifets BD, Chevaleyre V, Castillo PE. Interneuron activity controls endocannabinoid-mediated presynaptic plasticity through calcineurin. Proc Natl Acad Sci U S A. 2008; 105:10250–10255. [PubMed: 18632563]

Holt CE, Schuman EM. The central dogma decentralized: new perspectives on RNA function and local translation in neurons. Neuron. 2013; 80:648–657. [PubMed: 24183017]

Howlett AC, Barth F, Bonner TI, Cabral G, Casellas P, Devane WA, Felder CC, Herkenham M, Mackie K, Martin BR, et al. International Union of Pharmacology. XXVII. Classification of cannabinoid receptors. Pharmacol Rev. 2002; 54:161–202. [PubMed: 12037135]

Huang B, Wang W, Bates M, Zhuang X. Three-dimensional super-resolution imaging by stochastic optical reconstruction microscopy. Science. 2008; 319:810–813. [PubMed: 18174397]

Huang CC, Hsu KS. Local protein synthesis and GABAB receptors regulate the reversibility of long-term potentiation at murine hippocampal mossy fibre-CA3 synapses. J Physiol. 2004; 561:91–108. [PubMed: 15345751]

Huang YY, Li XC, Kandel ER. cAMP contributes to mossy fiber LTP by initiating both a covalently mediated early phase and macromolecular synthesis-dependent late phase. Cell. 1994; 79:69–79. [PubMed: 7923379]

Huber KM, Kayser MS, Bear MF. Role for rapid dendritic protein synthesis in hippocampal mGluR-dependent long-term depression. Science. 2000; 288:1254–1257. [PubMed: 10818003]

Irving AJ, Coutts AA, Harvey J, Rae MG, Mackie K, Bewick GS, Pertwee RG. Functional expression of cell surface cannabinoid CB(1) receptors on presynaptic inhibitory terminals in cultured rat hippocampal neurons. Neuroscience. 2000; 98:253–262. [PubMed: 10854756]

Jones EG, Powell TP. Synapses on the axon hillocks and initial segments of pyramidal cell axons in the cerebral cortex. J Cell Sci. 1969; 5:495–507. [PubMed: 5362338]

Jung H, Gkogkas CG, Sonenberg N, Holt CE. Remote control of gene function by local translation. Cell. 2014; 157:26–40. [PubMed: 24679524]

Jung KM, Sepers M, Henstridge CM, Lassalle O, Neuhofer D, Martin H, Ginger M, Frick A, DiPatrizio NV, Mackie K, et al. Uncoupling of the endocannabinoid signalling complex in a mouse model of fragile X syndrome. Nat Commun. 2012; 3:1080. [PubMed: 23011134]

Kano M, Ohno-Shosaku T, Hashimotodani Y, Uchigashima M, Watanabe M. Endocannabinoid-mediated control of synaptic transmission. Physiol Rev. 2009; 89:309–380. [PubMed: 19126760]

Katona I, Sperlagh B, Sik A, Kafalvi A, Vizi ES, Mackie K, Freund TF. Presynaptically located CB1 cannabinoid receptors regulate GABA release from axon terminals of specific hippocampal interneurons. J Neurosci. 1999; 19:4544–4558. [PubMed: 10341254]

Kelly A, Mullany PM, Lynch MA. Protein synthesis in entorhinal cortex and long-term potentiation in dentate gyrus. Hippocampus. 2000; 10:431–437. [PubMed: 10985282]

Klausberger T, Marton LF, O'Neill J, Huck JH, Dalezios Y, Fuentealba P, Suen WY, Papp E, Kaneko T, Watanabe M, et al. Complementary roles of cholecystokinin- and parvalbumin-expressing GABAergic neurons in hippocampal network oscillations. J Neurosci. 2005; 25:9782–9793. [PubMed: 16237182]

Klein ME, Castillo PE, Jordan BA. Coordination between Translation and Degradation Regulates Inducibility of mGluR-LTD. Cell Rep. 2015

Koenig E, Martin R, Titmus M, Sotelo-Silveira JR. Cryptic peripheral ribosomal domains distributed intermittently along mammalian myelinated axons. J Neurosci. 2000; 20:8390–8400. [PubMed: 11069946]

Martin KC, Casadio A, Zhu H, Yaping E, Rose JC, Chen M, Bailey CH, Kandel ER. Synapse-specific, long-term facilitation of aplysia sensory to motor synapses: a function for local protein synthesis in memory storage. Cell. 1997; 91:927–938. [PubMed: 9428516]

Moerke NJ, Aktas H, Chen H, Cantel S, Reibarkh MY, Fahmy A, Gross JD, Degterev A, Yuan J, Chorev M, et al. Small-molecule inhibition of the interaction between the translation initiation factors eIF4E and eIF4G. Cell. 2007; 128:257–267. [PubMed: 17254965]

Njoo C, Agarwal N, Lutz B, Kuner R. The Cannabinoid Receptor CB1 Interacts with the WAVE1 Complex and Plays a Role in Actin Dynamics and Structural Plasticity in Neurons. PLoS Biol. 2015; 13:e1002286. [PubMed: 26496209]

Palay SL, Palade GE. The fine structure of neurons. J Biophys Biochem Cytol. 1955; 1:69–88. [PubMed: 14381429]

Puighermanal E, Marsicano G, Busquets-Garcia A, Lutz B, Maldonado R, Ozaita A. Cannabinoid modulation of hippocampal long-term memory is mediated by mTOR signaling. Nat Neurosci. 2009; 12:1152–1158. [PubMed: 19648913]

Roland AB, Ricobaraza A, Carrel D, Jordan BM, Rico F, Simon A, Humbert-Claude M, Ferrier J, McFadden MH, Scheuring S, et al. Cannabinoid-induced actomyosin contractility shapes neuronal morphology and growth. Elife. 2014; 3:e03159. [PubMed: 25225054]

Santini E, Huynh TN, Klann E. Mechanisms of translation control underlying long-lasting synaptic plasticity and the consolidation of long-term memory. Prog Mol Biol Transl Sci. 2014; 122:131–167. [PubMed: 24484700]

Sekine Y, Zyryanova A, Crespillo-Casado A, Fischer PM, Harding HP, Ron D. Stress responses. Mutations in a translation initiation factor identify the target of a memory-enhancing compound. Science. 2015; 348:1027–1030. [PubMed: 25858979]

Shigeoka T, Jung H, Jung J, Turner-Bridger B, Ohk J, Lin JQ, Amieux PS, Holt CE. Dynamic Axonal Translation in Developing and Mature Visual Circuits. Cell. 2016; 166:181–192. [PubMed: 27321671]

Sonenberg N, Hinnebusch AG. Regulation of translation initiation in eukaryotes: mechanisms and biological targets. Cell. 2009; 136:731–745. [PubMed: 19239892]

Steward O, Ribak CE. Polyribosomes associated with synaptic specializations on axon initial segments: localization of protein-synthetic machinery at inhibitory synapses. J Neurosci. 1986; 6:3079–3085. [PubMed: 3093642]

Taylor AM, Berchtold NC, Perreau VM, Tu CH, Li Jeon N, Cotman CW. Axonal mRNA in uninjured and regenerating cortical mammalian axons. J Neurosci. 2009; 29:4697–4707. [PubMed: 19369540]

Tcherkezian J, Brittis PA, Thomas F, Roux PP, Flanagan JG. Transmembrane receptor DCC associates with protein synthesis machinery and regulates translation. Cell. 2010; 141:632–644. [PubMed: 20434207]

Twitchell W, Brown S, Mackie K. Cannabinoids inhibit N- and P/Q-type calcium channels in cultured rat hippocampal neurons. J Neurophysiol. 1997; 78:43–50. [PubMed: 9242259]

Wilhelm BG, Mandad S, Truckenbrodt S, Krohnert K, Schafer C, Rammner B, Koo SJ, Classen GA, Krauss M, Haucke V, et al. Composition of isolated synaptic boutons reveals the amounts of vesicle trafficking proteins. Science. 2014; 344:1023–1028. [PubMed: 24876496]

Xue S, Barna M. Specialized ribosomes: a new frontier in gene regulation and organismal biology. Nat Rev Mol Cell Biol. 2012; 13:355–369. [PubMed: 22617470]

Yin HH, Davis MI, Ronesi JA, Lovinger DM. The role of protein synthesis in striatal long-term depression. J Neurosci. 2006; 26:11811–11820. [PubMed: 17108154]

Yoon BC, Jung H, Dwivedy A, O'Hare CM, Zivraj KH, Holt CE. Local translation of extranuclear lamin B promotes axon maintenance. Cell. 2012; 148:752–764. [PubMed: 22341447]

Younts TJ, Chevaleyre V, Castillo PE. CA1 pyramidal cell theta-burst firing triggers endocannabinoid-mediated long-term depression at both somatic and dendritic inhibitory synapses. J Neurosci. 2013; 33:13743–13757. [PubMed: 23966696]

Yuan S, Burrell BD. Endocannabinoid-dependent long-term depression in a nociceptive synapse requires coordinated presynaptic and postsynaptic transcription and translation. J Neurosci. 2013; 33:4349–4358. [PubMed: 23467351]

Zhang X, Poo MM. Localized synaptic potentiation by BDNF requires local protein synthesis in the developing axon. Neuron. 2002; 36:675–688. [PubMed: 12441056]

## Highlights

- Presynaptic protein synthesis is required for long-term depression of GABA release
- iLTD involves cap-dependent translation in interneuron axons but not somata
- $CB_1$ activation enhances protein translation via mTOR signaling
- Eukaryotic ribosomes are present in inhibitory interneuron axons and terminals

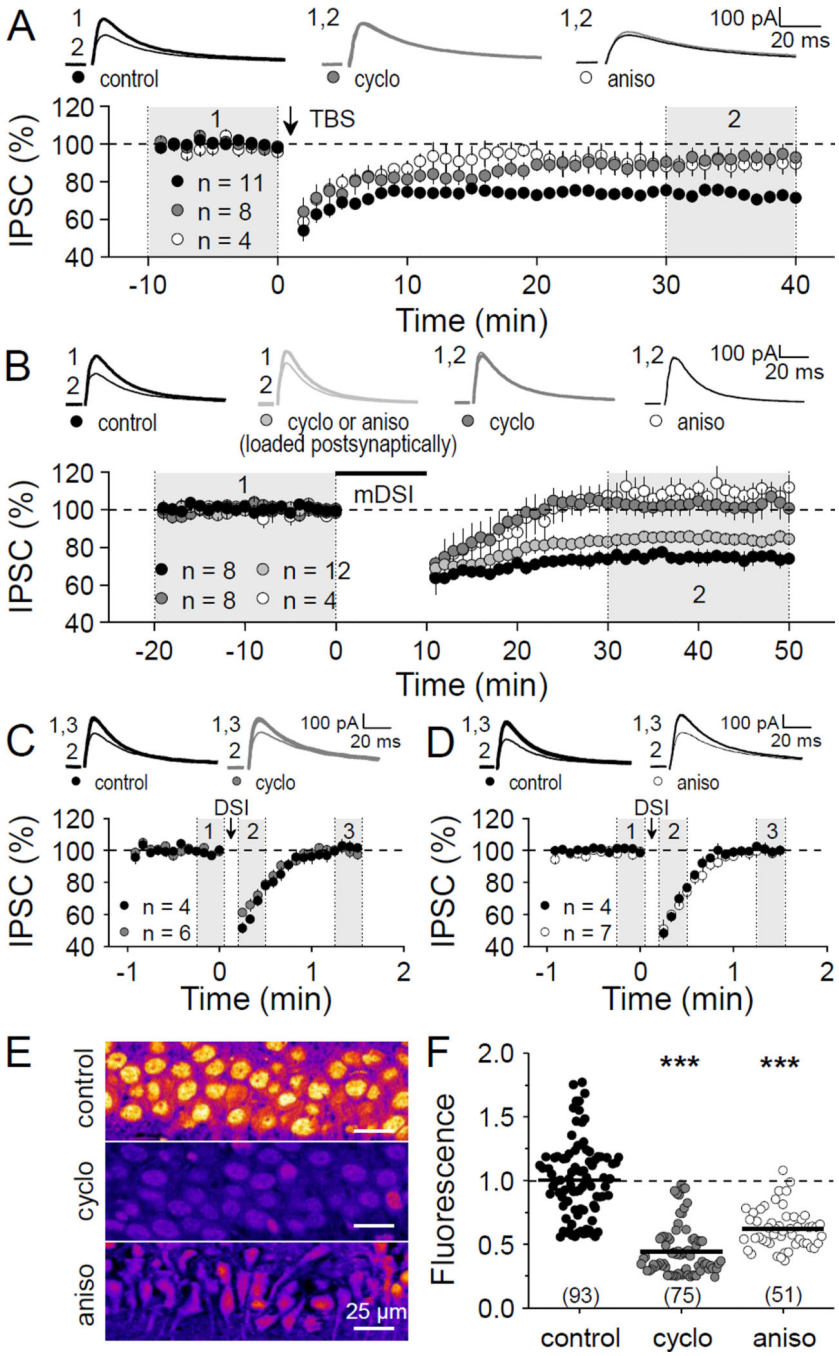


**Figure 1. Synaptically-induced iLTD involves protein synthesis**

**(A)** Whole-cell recordings from CA1 pyramidal cells in acute slices. Presynaptically-induced iLTD was blocked by acute bath application of cycloheximide (cyclo, 80 µM) or anisomycin (aniso, 20 µM) (washed-out after the induction). Arrow, TBS protocol. For all electrophysiology figures, representative traces (1) and (2) correspond to the gray shaded areas (1) and (2) in the summary time-course plots. Control: 73.1 ± 2.1% vs. cyclo: 91.4 ± 3.8% vs. aniso: 89.0 ± 5.1%; F[2,20] = 11.17646; p = 0.00055, one-way ANOVA. n = number of cells.

**(B)** Postsynaptically-induced iLTD was inhibited by acute bath application of cyclo (80 μM) or aniso (20 μM) (washed out after the induction). Except for control, cyclo (80 μM) or (20 μM) aniso was loaded postsynaptically via the patch pipette for all experiments. Black bar, mDSI protocol. Control: 74.3 ± 3.4% vs. cyclo or aniso loaded postsynaptically: 84.8 ± 2.2% vs. cyclo: 102.5 ± 5.2% vs. aniso: 109.6 ± 5.3%; $F[3,28] = 18.99148$; $p < 0.00001$, one-way ANOVA. Control vs. cyclo or aniso loaded postsynaptically; $p = 0.00135$, unpaired t-test.

**(C)** Short-term eCB-mediated plasticity elicited with DSI was not affected by cyclo (80 μM). Arrow, DSI protocol. Control: 63.6 ± 2.4% vs. cyclo: 69.5 ± 3.1%; $p = 0.18284$, unpaired t-test. Slices were exposed to cyclo for no more than 1 hr.

**(D)** Similar to panel C but for aniso (20 μM). Control: 68.3 ± 3.0% vs. aniso: 66.4 ± 2.8%; $p = 0.65988$, unpaired t-test.

**(E)** Cyclo (80 μM) and aniso (20 μM) blocks translation in slices as reflected by reduced FUNCAT signal in representative confocal images of the CA1 cell body layer.

**(F)** Summary data. FUNCAT fluorescence intensity, in arbitrary units, normalized to control. Control: 1.00 ± 0.03 (7 slices) vs. cyclo: 0.44 ± 0.02 (5 slices) vs. aniso: 0.62 ± 0.02 (3 slices); $F[2,216] = 116.10$; ***$p < 0.001$, one-way ANOVA;. Regions of interest (ROIs) were randomly selected from somata. Numbers in parenthesis refer to number of ROIs analyzed (i.e. 5 somas/image and ~3 images/slice).

(A–D): Data are shown as mean ± SEM.

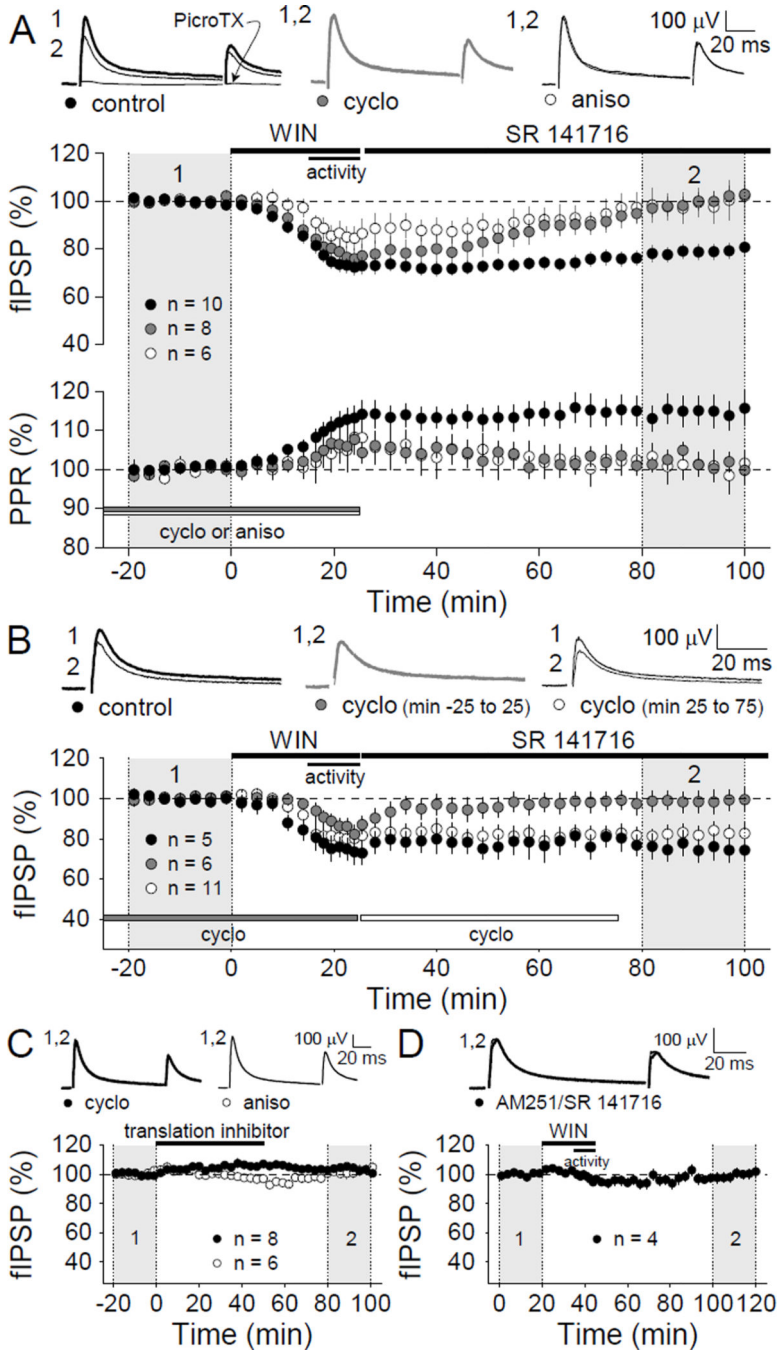


**Figure 2. Presynaptic $CB_1$-mediated iLTD requires translation during the induction-phase**

**(A)** fIPSP recordings in acute hippocampal slices. Top panel: chemically-induced iLTD (WIN 5 µM + activity, black bars) was blocked by bath application of cyclo (80 µM) or aniso (20 µM) (washed out after the induction). Control: 77.8 ± 2.4% vs. cyclo: 100.6 ± 3.9% vs. aniso: 99.2 ± 6.6%; F[2,21] = 11.30053; p = 0.00047, one-way ANOVA. SR 141716 (5 µM), a $CB_1$ inverse agonist/antagonist was bath applied after WIN to terminate $CB_1$ activation. Picrotoxin (bath applied at end of experiment) confirms fIPSPs were $GABA_A$ receptor-mediated. Bottom panel: translation inhibitors blocked the increased

paired-pulse ratio (PPR) associated with iLTD. Control: 112.5 ± 3% vs. cyclo: 102.2 ± 1.3% vs. aniso: 101.3 ± 3.4%; F[2,21] = 5.66567; p = 0.01077, one-way ANOVA. Gray and white bars signify presence of translation inhibitors. Data in both panels from same recordings. n = number of slices.

**(B)** Protein synthesis was required during the induction, but not maintenance, of iLTD. Slices were acutely exposed to cyclo (80 μM) during min −25 to 25 (gray bar) or min 25 to 75 (white bar). Control: 74.5 ± 5.2% vs. cyclo min −25 to 25: 98.6 ± 5.2% vs. cyclo min 25 to 75: 82.4 ± 4.2%; F[2,19] = 5.71536; p = 0.01002, one-way ANOVA.

**(C)** Neither cyclo (80 μM) nor aniso (20 μM) had a lasting impact on basal inhibitory synaptic transmission: cyclo: 105.1 ± 4.0% compared to baseline, p = 0.2378, paired t-test; aniso: 103.0 ± 4.1% compared to baseline; p = 0.48869, paired t-test. Inhibitors were bath applied for 50 min (black bar), as in panels A and B.

**(D)** AM251 (5 μM, n = 2) or SR 141716 (5 μM, n = 2) prevented iLTD: 101.2 ± 3.1% compared to baseline; p = 0.82567, paired t-test (AM251 and SR 141716 results pooled because there was no difference). Slices pre-incubated (>1 hr) and continuously perfused with $CB_1$ blockers.

Data are shown as mean ± SEM.

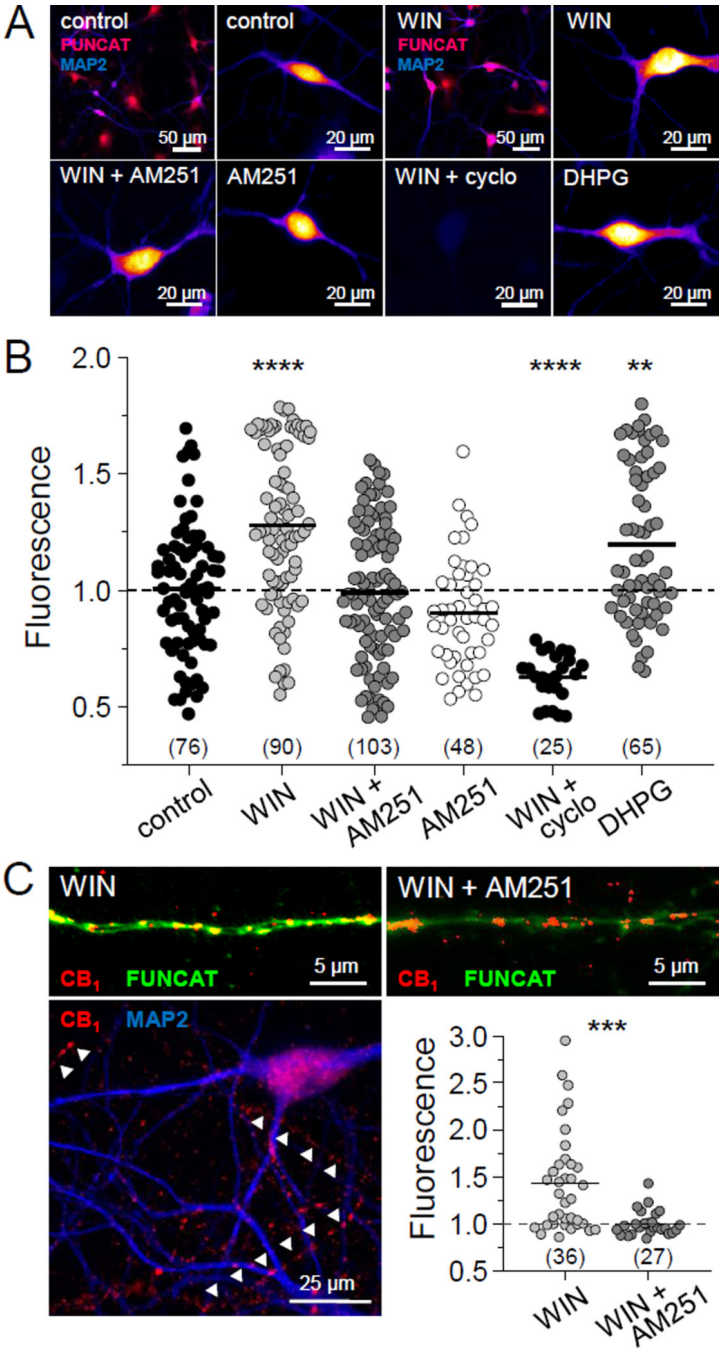


**Figure 3. $CB_1$ activation increases protein synthesis in neurons**

**(A)** Representative fluorescence images of FUNCAT signal acquired from primary hippocampal neurons (confirmed with MAP2 immunostaining which exclusively labels neurons) exposed for 25 min to vehicle control (DMSO), the $CB_1$ agonist WIN (5 µM), WIN and AM251 (both at 5 µM), AM251 alone (5 µM), WIN and cyclo (5 µM and 80 µM, respectively), or DHPG (50 µM, 10 min).

**(B)** Summary data. FUNCAT fluorescence intensity, in arbitrary units, normalized to control. Control (8 wells, 3 replicates): 1.00 ± 0.03 vs. WIN (7 wells, 3 replicates): 1.28

± 0.04 vs. WIN + AM251 (9 wells, 2 replicates): 0.99 ± 0.03 vs. AM251 alone (3 wells, 2 replicates): 0.90 ± 0.04 vs. WIN + cyclo (4 wells, 2 replicates): 0.63 ± 0.02 vs. DHPG (9 wells, 3 replicates): 1.20 ± 0.04 (9 wells, 3 replicates); F[5,401] = 28.09; **p <0.01, ****p < 0.0001, one-way ANOVA. ROIs were generated from neuronal somata and neurites using MAP2. Numbers in parentheses refer to number of images analyzed (i.e. 2–8 neurons/image and ~5 images/well).

**(C)** Top panels: representative fluorescence images of FUCAT signal acquired from putative axons under $CB_1$-positive puncta exposed to WIN (5 μM) and WIN + AM251 (both at 5 μM). Bottom left: wide-field image of a neuron immunostained with $CB_1$ and MAP2. Arrowheads indicate putative axons containing $CB_1$ but lacking MAP2 staining. Right: summary data of FUNCAT fluorescence intensity, in arbitrary units, normalized to WIN + AM251. WIN (7 wells, 2 replicates): 1.42 ± 0.09 vs. WIN + AM251 (6 wells, 2 replicates): 1.00 ± 0.02; U = 202, ***p <0.001, Mann Whitney. Numbers in parentheses refer to number of images analyzed (i.e. 1–2 neurons/image and ~5 images/well).

Data represent mean ± SEM.

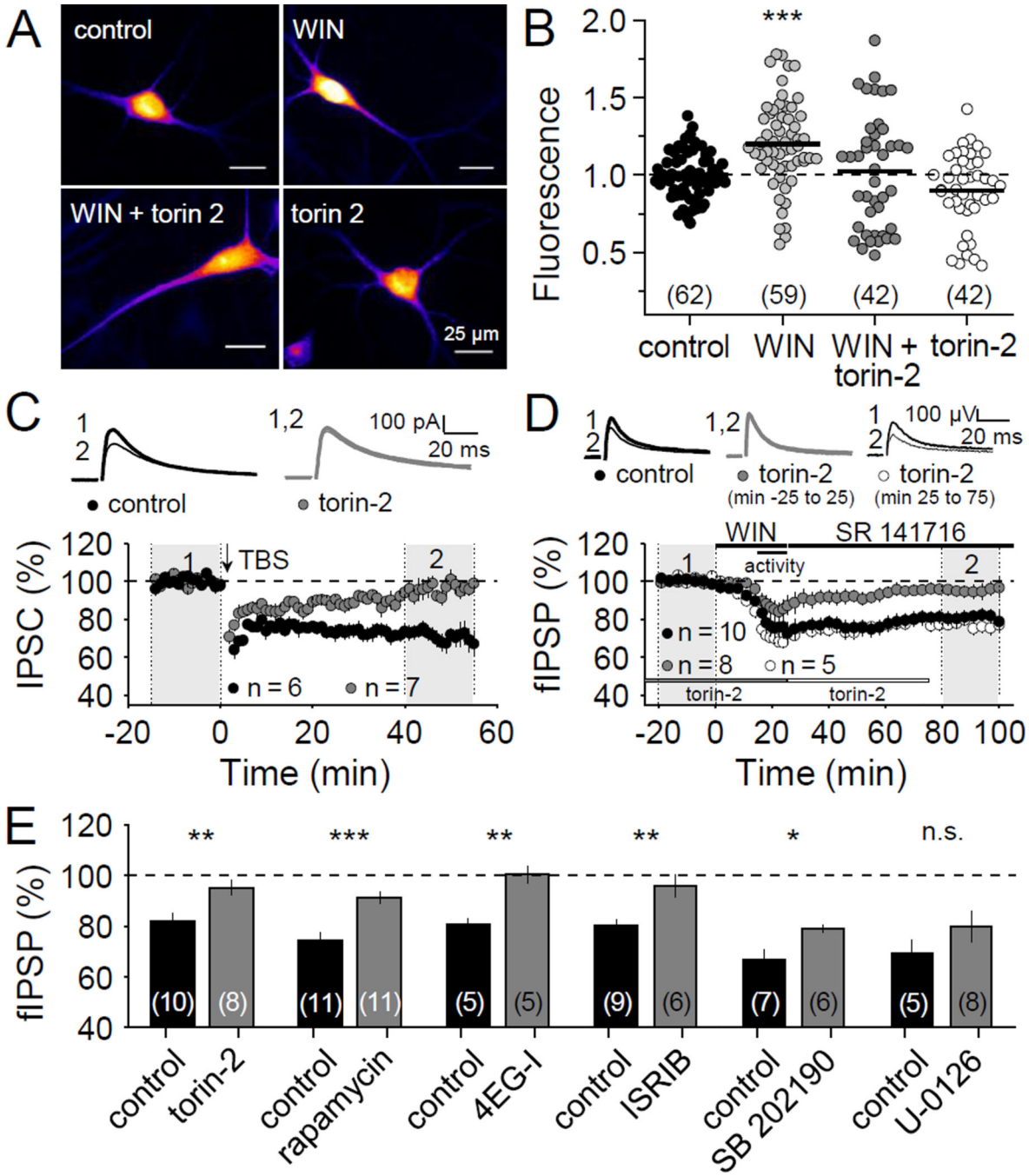


**Figure 4. $CB_1$-mediated iLTD recruits the mTOR pathway**

**(A)** Representative fluorescence images of FUNCAT signal acquired from cultured primary hippocampal neurons exposed for 25 min to vehicle control (DMSO), WIN (5 µM), WIN (5 µM) and the mTOR inhibitor torin-2 (100 nM), and torin-2 alone (100 nM).

**(B)** Summary data. FUNCAT fluorescence intensity, in arbitrary units, normalized to control. Control (9 wells, 4 replicates): 1.00 ± 0.02 vs. WIN (7 wells, 3 replicates): 1.20 ± 0.04 vs. WIN + torin-2 (5 wells, 2 replicates): 1.02 ± 0.06 vs. torin-2 alone (6 wells, 2 replicates): 0.90 ± 0.04. F[3,201] = 11.90; ***p<0.001, one-way ANOVA. Numbers in

parentheses refer to number of images analyzed (i.e. 2–8 neurons/image and ~5 images/well).

**(C)** Whole-cell recordings in acute hippocampal slices. Presynaptically-induced TBS-iLTD was abolished by torin-2 (100 nM). Control: 70.8 ± 4.3% vs. torin-2: 94.0 ± 3.0%; p = 0.00083, unpaired t-test. Slices pre-incubated (>1 hr) and continuously perfused with torin-2.

**(D)** fIPSP recordings in acute hippocampal slices. mTOR was required during the induction, but not maintenance, of chemical-iLTD. Slices were acutely exposed to torin-2 (100 nM) during min −25 to 25 or min 25 to 75. Control: 81.8 ± 3.3% vs. torin-2 min −25 to 25: 95.2 ± 3% vs. torin-2 min 25 to 75: 72.5 ± 4.6%; F [2,19] = 8.45658; p = 0.00236, one-way ANOVA.

**(E)** Summary data for fIPSP recordings showing that mTOR and cap-dependent translation are required for chemical-iLTD. Data from panel D were replotted for comparison. iLTD was blocked in slices acutely exposed (washed out after induction) to the mTOR inhibitor rapamycin (100 nM) (control: 74.2 ± 3.4% vs. rapamycin: 91.3 ± 2.3; p = 0.00054) and the cap-dependent translation inhibitor 4EGI-1 (1 μM) (control: 80.5 ± 2.6% vs. 4EGI-1: 100.3 ± 3.4%; p = 0.00169). ISRIB (1 μM), a different cap translation inhibitor, blocked iLTD in slices pre-incubated (>1 hr) and continuously perfused (control: 80.1 ± 2.4% vs. ISRIB: 95.8 ± 4.4%; p = 0.00408). iLTD was partially blocked in slices acutely exposed (washed out after induction) to the p38 MAPK inhibitor SB 202190 (10 μM) (control: 66.7 ± 3.9 vs. SB 202190: 79 ± 1.2%; p = 0.01661) but not the MAPK/ERK inhibitor U-0126 (10 μM) (control: 69.2 ± 5.3% vs. U-0126: 79.8 ± 6.1%; p = 0.13075). The inactive form of U-0126, U-0124, was used as control. Unpaired t-tests.

Data are shown as mean ± SEM.

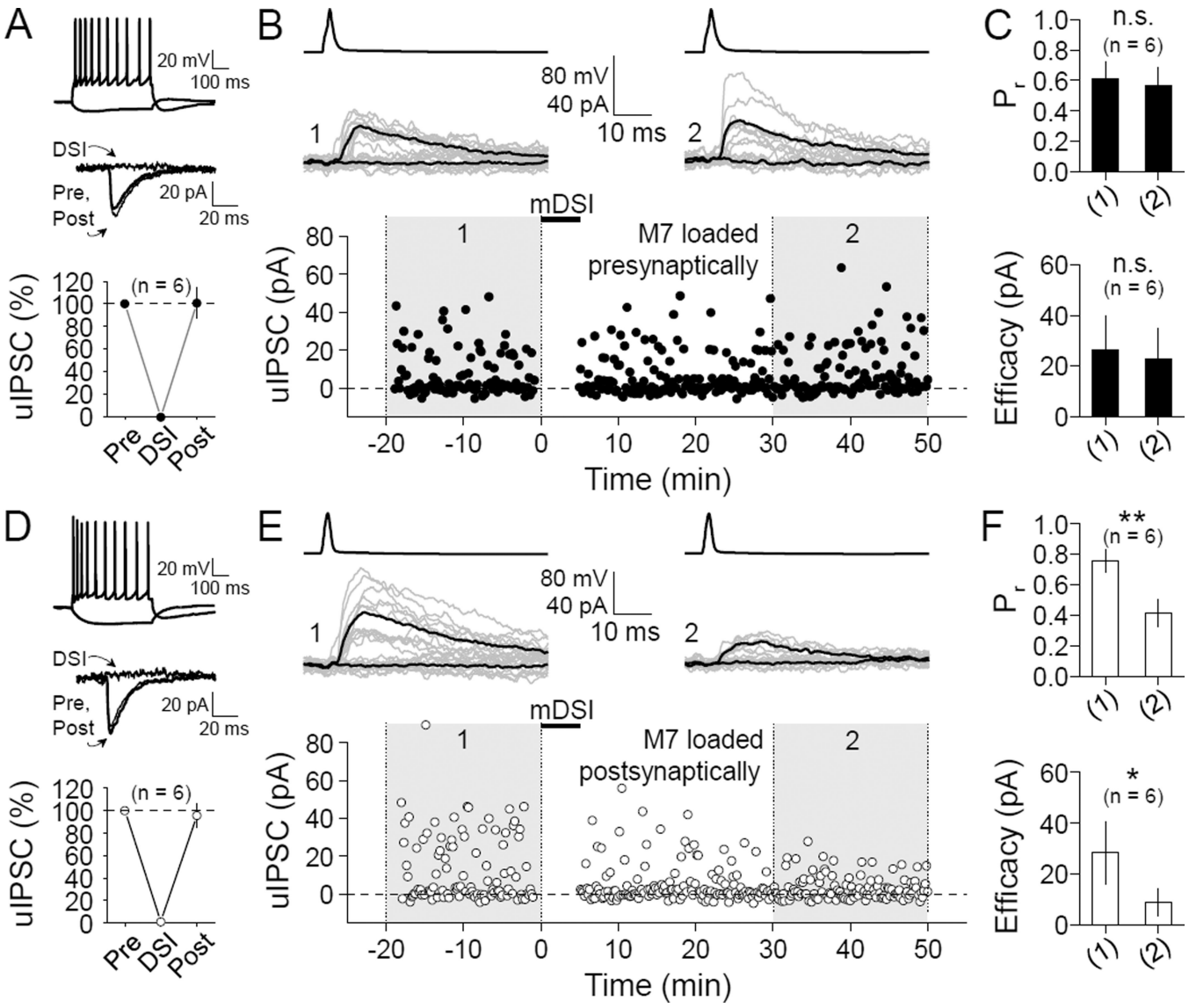


**Figure 5. Presynaptic cap-dependent protein synthesis is essential for iLTD**

**(A–C)** Paired recordings in which M7 was loaded presynaptically via the patch pipette.

**(A)** Top: regular-spiking action potential firing pattern characteristic of DSI sensitive and thus $CB_1$-expressing interneurons. Middle: Representative traces collected before, during, and after DSI. Bottom: DSI summary data. DSI: −0.8 ± 6.2% compared to baseline; p <0.00001, paired t-test. uIPSC (unitary IPSC).

**(B)** Representative time course plot for an attempted iLTD experiment in which M7 (250 μM) was loaded presynaptically into the interneuron for 86 min prior to inducing iLTD. Black bar, mDSI protocol. Presynaptic action potentials (averaged) and corresponding evoked uIPSCs are shown (example responses and failures in gray; averaged responses and failures in black).

**(C)** Summary data. (1) and (2) refer to baseline and after iLTD induction, respectively (see gray shaded areas in panel B). $P_r$ during baseline: 0.62 ± 0.11 vs. after iLTD induction: 0.56 ± 0.12; p = 0.56546, paired t-test. Efficacy during baseline: 26.4 ± 13.2 pA vs. after iLTD

induction: 23.0 ± 11.9 pA; p = 0.48395, paired t-test. See Figure S2A for time-course plots of summary data. **(D–F)** Paired recordings in which M7 was loaded postsynaptically via the patch pipette.

**(D)** Similar to panel A. DSI: 1.1 ± 3.9% compared to baseline; p <0.00001, paired t-test. Magnitude of DSI was not significantly different from that in panel A; p = 0.90793, unpaired t-test.

**(E)** Similar to panel B, but M7 (250 μM) was loaded postsynaptically into the CA1 pyramidal cell for 40 min prior to inducing iLTD.

**(F)** Summary data. $P_r$ during baseline: 0.75 ± 0.08 vs. after iLTD induction: 0.42 ± 0.09; p = 0.00193, paired t-test. Efficacy during baseline: 28.4 ± 12.3 pA vs. after iLTD induction: 8.9 ± 5.3 pA; p = 0.04314, paired t-test. The baseline $P_r$ and synaptic efficacy were not different between M7 loaded presynaptically and postsynaptically experiments (p = 0.30708 and p = 0.70520, respectively, unpaired t-tests). See Figure S2B,C for M7 loaded postsynaptically positive control.

Data are shown as mean ± SEM.

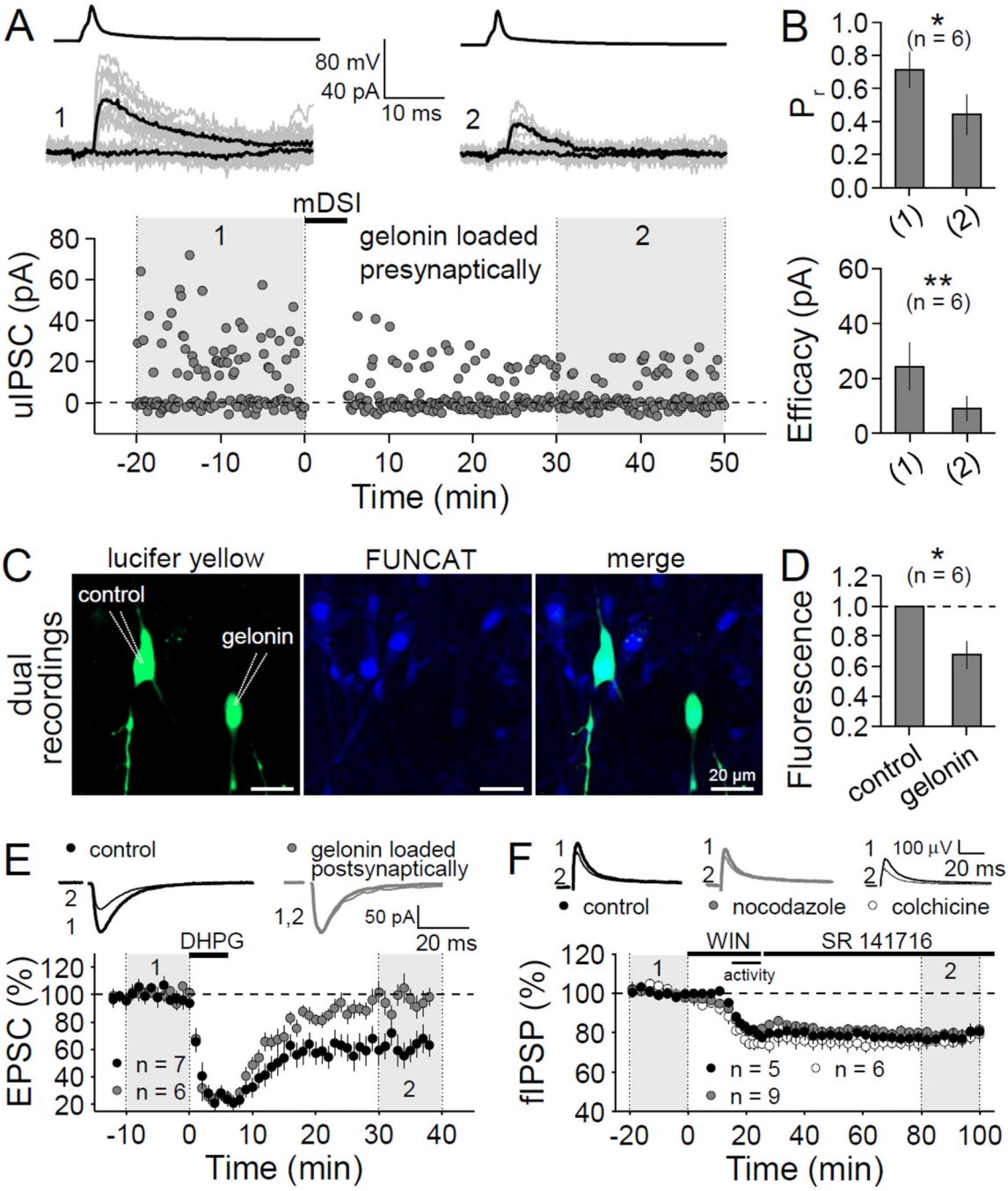


**Figure 6. Somatic protein synthesis is dispensable for iLTD**

**(A)** Representative iLTD time course plot for a paired recording in acute hippocampal slices in which gelonin (3 µM) was loaded presynaptically into the CA1 interneuron for ~100 min prior to inducing iLTD. Black bar, mDSI protocol.

**(B)** Summary data. $P_r$ during baseline: 0.71 ± 0.10 vs. after iLTD induction: 0.44 ± 0.12; p = 0.02257, paired t-test. Efficacy during baseline: 24.3 ± 8.7 pA vs. after iLTD induction: 9.0 ± 4.5 pA; p = 0.01699, paired t-test. The baseline $P_r$ and synaptic efficacy were not statistically different between gelonin loaded presynaptically and M7 loaded

postsynaptically, which served as control (p = 0.64124 and p = 0.98827, respectively, unpaired t-tests) (**c.f.** Figure 5F).

**(C)** Gelonin (3 μM) blocks somatic translation at the single-cell level in acute hippocampal slices. Left panel: representative confocal images of two neighboring CA1 interneurons that were patched near-simultaneously and loaded via the patch-pipette with the morphological dye, lucifer yellow (2 mM). Gelonin (3 μM) was also loaded into the cell on the right for ~30 min. The pipettes were gently withdrawn. Slices were then processed for FUNCAT. Middle panel: FUNCAT signal from the same slice. Right panel: merged images.

**(D)** Summary data and FUNCAT quantification (fluorescence intensity, in arbitrary units, normalized to control) for dual recordings. Cells were loaded for 30.0 ± 2.3 min. Control: 1.0 ± 0.0 vs. gelonin: 0.67 ± 0.09, p=0.0313, Wilcoxon matched-pairs signed rank test. Homogenous ROIs (n = 2) were selected from each neuronal somata (n = 6 slices).

**(E)** Whole-cell recordings in which gelonin (3 μM) loaded postsynaptically into CA1 pyramidal cells blocked chemically-induced mGluR-LTD (DHPG, 50 μM, 5 min, black bar). Control: 62.2 ± 8.1% vs. gelonin: 98.2 ± 6.4%; p = 0.00221, unpaired t-test. Gelonin was loaded for 32.0 ± 2.3 min before DHPG application.

**(F)** Field recordings in which the microtubule depolymerizing compounds nocodazole (20 μM) and colchicine (100 μM) did not affect chemical iLTD. Control: 77.2 ± 3.1% vs. colchicine: 76.0 ± 2.5% vs. nocodazole: 79.8 ± 2.0%; F[2,17] = 0.72626; p = 0.49813, one-way ANOVA. Slices were pre-incubated in colchicine and nocodazole for >2.5 hrs (usually ~ 4 hrs, up to 5 and 8 hrs, respectively) and continuously perfused. See Figure S4 for nocodazole positive control.

Data are shown as mean ± SEM.

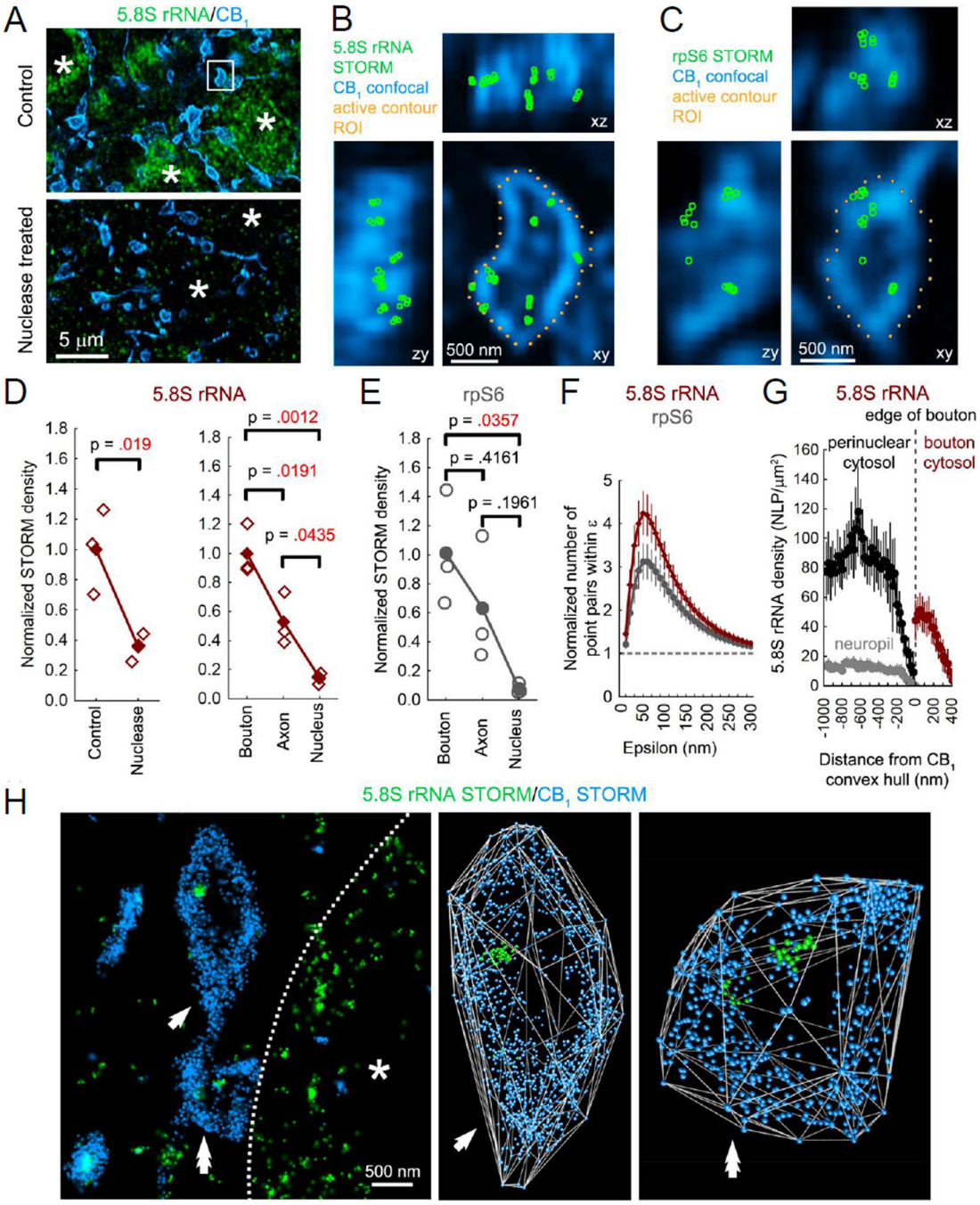


**Figure 7. Ribosomes are present in $CB_1$-expressing interneuron axons and terminals**

**(A)** Fixed mouse hippocampal slices were immunostained against 5.8S rRNA using the monoclonal Y10b antibody (green) and $CB_1$ antibody (blue). Deconvolved confocal image of 5.8S rRNA immunostaining in CA1 cell body layer reveals heavily labeled perinuclear cytoplasm of pyramidal cells (asterisks). Note the characteristically dense meshwork of axons and preterminal axon segments expressing $CB_1$ receptors (box). Compared with control, sections pretreated with nuclease enzymes had significantly less 5.8S rRNA

immunolabeling (quantified in panel D), confirming the specificity of the antibody and labeling procedure.

**(B)** Representative maximum intensity volume view of correlated confocal and 3D-STORM microscopy images shows 5.8S rRNA immunolabeling inside a $CB_1$-expressing axon terminal (panel A, white box). An area within $CB_1$-expressing axon terminals was selected from the central confocal slice using an unbiased active contour algorithm (gold outline in xy plane of panels B and C). The number of STORM localization points within these ROIs was used to calculate density values for each bouton.

**(C)** Similar to panel B, but for ribosomal protein, rpS6. Same imaging modality as in panel B.

**(D)** Left panel: pretreatment with nuclease enzymes decreased STORM localization point density in $CB_1$-expressing axon terminals (n = 28 ± 2 standard deviations, unpaired t-test). Right panel: Interneuron axon terminals (n = 29 ± 1) contained significantly more ribosomal labeling compared to preterminal axon segments (n = 13 ± 3) and pyramidal cell nuclei (n = 4), representing background staining, one-way ANOVA. Each graph shows raw data normalized to control axon terminals (n = 3 mice per condition).

**(E)** Similarly, rpS6 immunopositive STORM labeling density was significantly higher in axon terminals (n = 21 ± 3) than background staining in nuclei (n = 4), one-way ANOVA. Preterminal segments (n = 13 ± 2).

**(F)** Nanoscale spatial distribution of 5.8S rRNA and rpS6 immunolabeling was virtually identical (**c.f.** Figure S6A–C). Maximal clustering between pairs of localization points occurred near ~50 nm (note apparent clustering of points in panels B and C). ε refers to the Euclidian distance between point pairs that are confined by the active contour border. The y-axis refers to the number of point pairs separated by less than ε normalized to a randomized distribution of such point pairs for each distance. Filled symbols represent the mean and error bars the 95% confidence interval.

**(G)** Dual-channel 3D-STORM imaging of $CB_1$ and 5.8S rRNA immunolabeling shows high density of ribosomal material at the inner plasma membrane surface of $CB_1$-expressing axon terminals (n = 25 boutons, 2 mice, representative images in panel H). The outer surface of the bouton was largely devoid of 5.8S rRNA immunolabeling. The signal was present at low density in surrounding neuropil and accumulated in neighboring cells with distance from the terminals. Filled symbols are mean ± 95% confidence interval. NLP, number of localization points.

**(H)** Dual-channel 3D volume renderings of two adjacent $CB_1$-expressing axon terminals (single arrowhead and double arrowhead) demonstrate 5.8S rRNA immunolabeling inside the convex hull fit to $CB_1$ localization points (silver lines). Dotted line indicates neighboring postsynaptic neuron cell body (asterisk).